

Remotely preparing optical Schrödinger cat states via homodyne detection in nondegenerate triple-photon spontaneous downconversion

Miaomiao Wei¹, Huatang Tan^{1,*} and Qiongyi He²

¹ Department of Physics, Huazhong Normal University, Wuhan 430079, China

² State Key Laboratory for Mesoscopic Physics, School of Physics, Frontiers Science Center for Nano-Optoelectronics, and Collaborative Innovation Center of Quantum Matter, Peking University, Beijing 100871, China

* Author to whom any correspondence should be addressed.

E-mail: tht@mail.ccnu.edu.cn and qiongyihe@pku.edu.cn

Abstract. Optical downconversion is a key resource for generating nonclassical states. Very recently, direct nondegenerate triple-photon spontaneous downconversion (NTPSD) with bright photon triplets and strong third-order correlations has been demonstrated in a superconducting device [Phys. Rev. X **10**, 011011 (2020)]. Besides, linear and nonlinear tripartite entanglement in this process have also been predicted [Phys. Rev. Lett **120**, 043601 (2018); Phys. Rev. Lett. **125**, 020502 (2020)]. In this paper, we consider the generation of nonclassical optical quantum superpositions and investigate nonlinear quantum steering effects in NTPSD. We find that large-size Schrödinger cat states of one downconverted mode can be achieved when the other two modes are subjected to homodyne detection. Also, a two-photon Bell entangled state can be generated when only one mode is homodyned. We further reveal that such ability of remote state steering originates from nonlinear quantum steerable correlations among the triplets. This is specifically embodied by the seeming violation of the Heisenberg uncertainty relation for the inferred variances of two noncommuting higher-order quadratures of downconverted modes, based on the outcomes of homodyne detection on the other mode, i.e., nonlinear quantum steering, compared to original Einstein-Podolsky-Rosen steering. Our results demonstrate non-Gaussian nonclassical features in NTPSD and would be useful for the fundamental tests of quantum physics and implementations of optical quantum technologies.

Keywords: Schrödinger cat states, two-photon Bell entangled states, nonlinear quantum steering, nondegenerate triple-photon spontaneous downconversion

1. Introduction

The generation of Schrödinger's cat state [1] — a quantum superposition of macroscopically distinct states — always attracts intense research interests because that

it is important not only for understanding fundamentals of quantum mechanics [2–7], such as quantum decoherence [5], but also for a number of quantum technologies [8–14]. To date, Schrödinger’s cat states have been experimentally realized in the systems of e.g. atoms [15–19] and photons [20–24]. In particular, the creation of optical cat states by photon subtraction on squeezed light has been demonstrated [21–24], which, however, only generates small-size cat states and moreover depends on single-photon resolved detection. In this situation, when taking into account that homodyne detection has become a relatively mature and high-efficiency technology, it is therefore interesting to generate large-size optical cat states via homodyne detection [25].

Distinct from second-order twin-photon downconversion which yields Gaussian-state nonclassical light, three-order triple-photon downconversion can create photon triplets in nontrivial non-Gaussian states [26–38], e.g., higher-order squeezing [28] which enables error correction in quantum computing [34]. As we know, Non-Gaussian states, which may exhibit negative Wigner functions and genuine nonclassicality, has advantageous over Gaussian counterparts in e.g. implementing universal quantum computation [39]. Spontaneous triple-photon downconversion has been observed in optical fiber but with weak generation rate [40]. Very recently, direct NTPSD with bright photon triplets and strong third-order correlations has been achieved with a superconducting cavity [41]. This achievement makes the triplet-photon generation a potential approach to the generation of optical tripartite entanglement and also excites research interests in studying non-Gaussian quantum properties in the process. For instance, three-mode linear-quadrature entanglement in NTPSD [35] was analyzed by González et al., while Agustí et al. found that tripartite genuine non-Gaussian entanglement exists in the process [37]. In addition, some Gaussian and non-Gaussian quantum effects was also revealed by Zhang et al. in Ref. [38].

In this work, we intend to investigate nonlinear quantum steering effect in NTPSD and its application to the remote generation of optical nonclassical quantum superpositions. Quantum steering reflects the ability of quantum nonlocality to steer quantum states of a particle which is entangled with another remote particle subjected to local measurements [42–45]. One can exploit quantum steering to remotely prepare desirable quantum states, e.g., quantum quadrature squeezed states [46, 47], via homodyne detection. Quantum steering has been realized in a variety of systems [48–53], whereas for continuous-variable systems only Gaussian steering has been reported.

We find in this paper that the inferred variances of two noncommuting higher-order quadratures of downconverted modes, conditioned on the linear-quadrature measurements of another distant mode, can seemingly violate the Heisenberg uncertainty relation, indicating nonlinear quantum steering effect, in comparison to original Einstein-Podolsky-Rosen steering [42, 54]. We show that such kind of nonlinear quantum steerable correlations enable the remote generation of large-size single-mode optical Schrödinger cat states with high fidelity and two-mode Bell entangled states via homodyne detection. These non-Gaussian optical quantum superpositions exhibit negative Wigner functions, showing strong non-Gaussian nonclassicality. Our results

reveal nontrivial non-Gaussian nonclassical features in NTPSD and would be useful for the fundamental tests of quantum physics and implementations of quantum technologies.

2. System

We consider a NTPSD process in which a pump photon of high frequency ω_p is simultaneously down-converted into three low frequency photons, with frequencies ω_a , ω_b and ω_c satisfying the energy conservation $\omega_p = \omega_a + \omega_b + \omega_c$. When taking into account

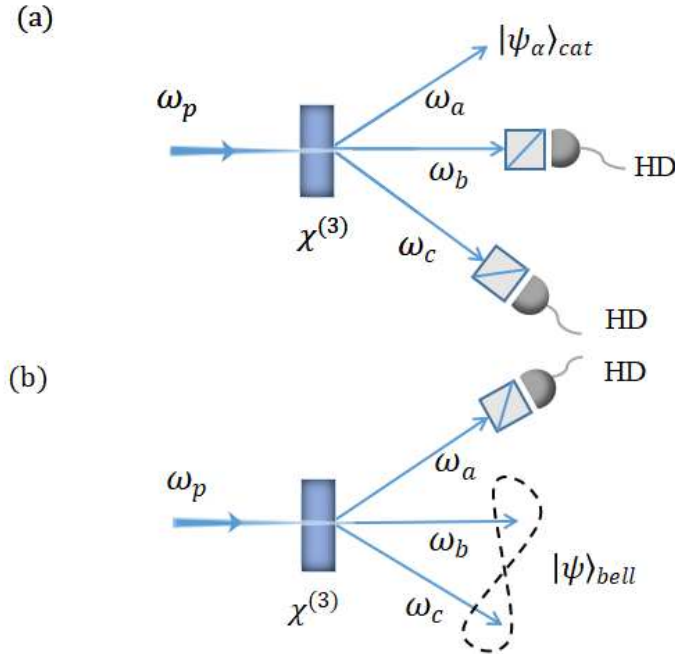


Figure 1. Schematic diagram for remotely generating optical quantum superpositions by homodyne detection in a NTPSD process in which a high-frequency pump photon (with frequency ω_p and in a coherent state $|\alpha_p\rangle$) is simultaneously downconverted into a triplet (denoted by a, b, c) of frequencies ω_a, ω_b and ω_c . (a) By homodyning the downconverted modes b and c , the third mode c is steered into a size-adjustable Schrödinger cat state $[|\psi_\alpha\rangle_{\text{cat}} = (|i\alpha\rangle + |-i\alpha\rangle)/\sqrt{2(1+e^{-2|\alpha|^2})}]$. (b) When only one mode (e.g. the mode a) is homodyned, the other two modes are projected into a two-photon Bell entangled state $[|\psi\rangle_{\text{bell}} = (|0_b, 0_c\rangle + |1_b, 1_c\rangle)/\sqrt{2}]$. The abbreviation “HD” stands for homodyne detection.

of pump depletion, we can describe this process by using the following Hamiltonian ($\hbar = 1$)

$$\hat{H}_q = i\chi^{(3)}(\hat{a}^\dagger\hat{b}^\dagger\hat{c}^\dagger\hat{p} - \hat{a}\hat{b}\hat{c}\hat{p}^\dagger), \quad (1)$$

where $\chi^{(3)}$ is the third-order nonlinear coupling. The annihilation operators $\hat{p}, \hat{a}, \hat{b}$, and \hat{c} and their conjugates denote the pump mode and three down-converted modes, respectively. Experiments have realized optical NTPSD in optical fiber [40], with small triplet generation rate. While in the microwave domain, Chang et al. have very recently

achieved direct NTPSD by using a flux-pumped superconducting parametric cavity and also observed strong three-body correlations among the triple modes [41].

Given initial vacua of the triplets $|0_a, 0_b, 0_c\rangle$ and a coherent state of the pump mode $|\alpha_p\rangle = e^{-|\alpha_p|^2/2} \sum_{n_p} \alpha_p^{n_p} |n_p\rangle / \sqrt{n_p!}$, with the amplitude α_p , the state's evolution of the whole system is governed by

$$\frac{d|\psi(t)\rangle_{abcp}}{dt} = -i\hat{H}_q|\psi(t)\rangle_{abcp}, \quad (2)$$

By expanding the state vector in the Fock space $\{|n_a, n_b, n_c, n_p\rangle\}$, $|\psi(t)\rangle_{abcp} = \sum_n c_{n,n_p}(t)|n_a, n_b, n_c, n_p - n\rangle$, with $n_{a,b,c} = n$ for the photon-triplet generation, the amplitude $c_{n,n_p}(t)$ and thus the state vector can be obtained numerically. Since we are only interested the photon triplets, the reduced state $\hat{\rho}_{abc}(t)$ of the triplets can be obtained by tracing out the pump mode.

3. Optical quantum superpositions

With the density matrix $\hat{\rho}_{abc}$ of the triplets, we can study remotely steering quantum states of downconverted modes via homodyne detection on the linear quadratures $\hat{X}_o = (\hat{o} + \hat{o}^\dagger)/\sqrt{2}$ ($o = a, b, c$) of the other modes. We first investigate the state of the mode a when simultaneously homodyning the quadratures \hat{X}_b and \hat{X}_c . Conditioned on the measurement outcomes x_b and x_c , the density operator $\hat{\rho}_a^{\text{con}}(x_b, x_c)$ can be formally given by

$$\hat{\rho}_a^{\text{con}}(x_b, x_c) = \frac{\hat{\rho}_a^{\text{con}}(x_b, x_c)}{\text{Tr}_a[\hat{\rho}_a^{\text{con}}(x_b, x_c)]}, \quad (3)$$

where $\hat{\rho}_a^{\text{con}}(x_b, x_c) = \text{Tr}_{bc}[(\hat{\mathcal{M}}_{bc} \otimes \hat{I}_a)\hat{\rho}_{abc}(\hat{I}_a \otimes \hat{\mathcal{M}}_{bc})]$ and $\hat{\mathcal{M}}_{bc} = |x_b, x_c\rangle\langle x_b, x_c|$ which can be calculated in the Fock space with $\langle x_o | n_o \rangle = \frac{1}{\pi^{1/4}} \frac{1}{\sqrt{2^{n_o} n_o!}} e^{-x_o^2/2} H_{n_o}(x_o)$, H_n the Hermite polynomial of order n . The superscript ‘‘con’’ stands for ‘‘conditional’’ and similarly hereinafter.

We consider the Wigner function $W_a^{\text{con}}(x_a, p_a)$ of the density matrix $\hat{\rho}_a^{\text{con}}(x_b, x_c)$, obtained by performing Fourier transform on the characteristic function defined via $\chi_a(\xi) = \text{Tr}[e^{\xi\hat{a}^\dagger - \xi^*\hat{a}}\hat{\rho}_a^{\text{con}}(x_b, x_c)]$. In Fig.2, the density plots of the Wigner function $W_a^{\text{con}}(x_a, p_a)$ for the measurement outcomes $x_c = 0$ and $x_b = \{3, 4, 5, 6\}$ are presented at the interaction time $\alpha_p \chi^{(3)} t = 0.3$. It shows that the Wigner function exhibits obvious negativity, indicating strong non-Gaussian nonclassicality. In Fig.3 (a), we plot the the fidelity $F_a = \text{Tr}[\sqrt{\sqrt{\hat{\rho}_\alpha}\hat{\rho}_a^{\text{con}}\sqrt{\hat{\rho}_\alpha}}]$, with respect to the ideal cat state $\hat{\rho}_\alpha = |\psi_\alpha\rangle_{\text{cat}}\langle\psi_\alpha|$ and

$$|\psi_\alpha\rangle_{\text{cat}} = \frac{1}{\sqrt{2(1 + e^{-2|\alpha|^2})}}(|i\alpha\rangle + |-i\alpha\rangle). \quad (4)$$

We see that high fidelity can be achieved. For instance, $F_a \approx 0.98$ for the amplitude $\alpha \approx 1.2$. The downconverted mode a is thus steered by the measurement into a cat state

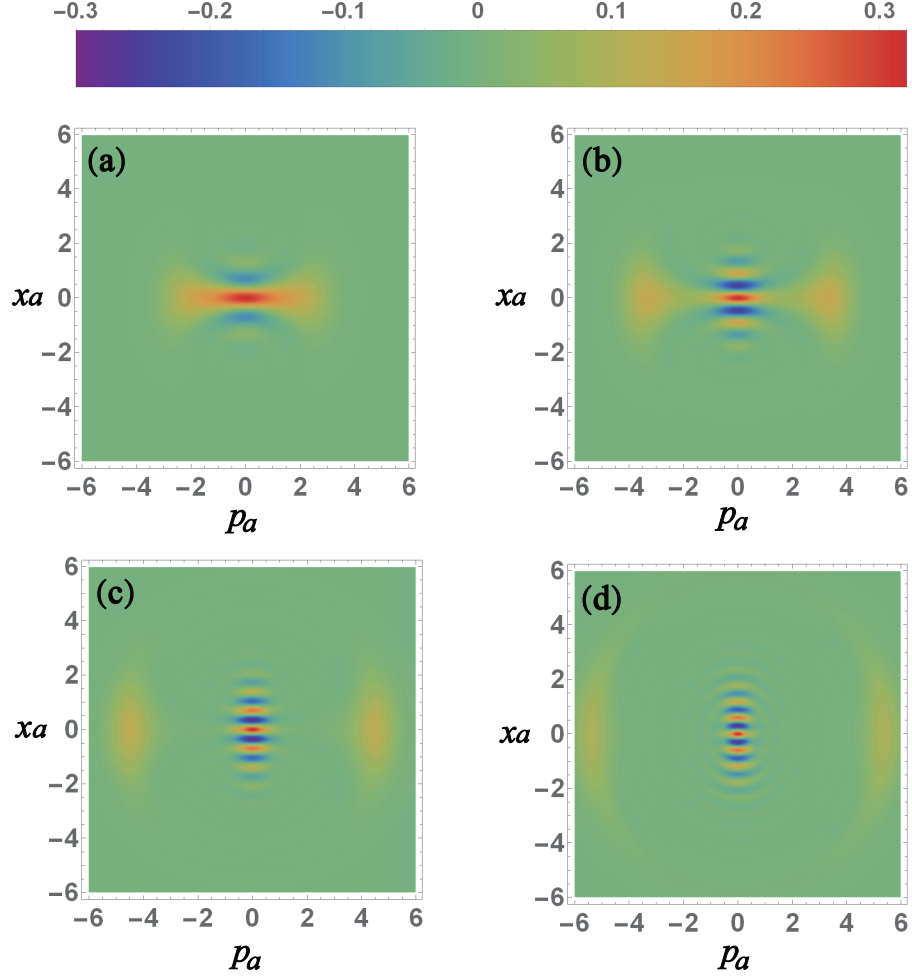


Figure 2. The density plots of the Wigner function $W_a^{\text{con}}(x_a, p_a)$ for the measurement results $x_c = 0$ and (a) $x_b = 3$, (b) $x_b = 4$, (c) $x_b = 5$, and (d) $x_b = 6$. The interaction time $\alpha_p \chi^{(3)} t = 0.3$ and pump amplitude $\alpha_p = \sqrt{10}$.

remotely. Further, the size of the cat states can be adjustable and, as shown explicitly, it grows up but still with high fidelity when the measurement outcome increases from $x_b = 3$ to $x_b = 6$. For example, high-fidelity cat state ($F_a \approx 0.95$) with large amplitude $\alpha \approx 3.2$ can be achieved. We see from Fig.3 (b) the purity of the state $\hat{\rho}_a^{\text{con}}$, defined by $P_a = \text{Tr}[(\hat{\rho}_a^{\text{con}})^2]$, is almost equal to unit and just slightly decreases as x_b increases from $x_b = 3$. Fig. 2 also shows that the two peaks in p_a become more separated with larger values of the outcome x_b , representing larger size of the created cats but still with stronger nonclassicality \mathcal{N}_a and macroscopicity \mathcal{M}_a , as shown in Fig.3 (b), which defined, respectively, by [55]

$$\mathcal{N}_a \equiv \int (|W(\beta, \beta^*)| - W(\beta, \beta^*)) d^2 \beta, \quad (5)$$

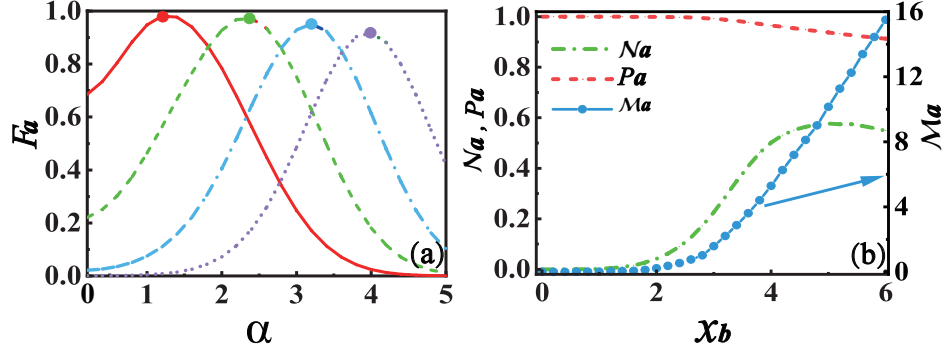


Figure 3. (a) The fidelity F_a between the achieved state $\hat{\rho}_a^{\text{con}}$ and the ideal cat state $|\psi_a\rangle$ as the function of the cat-state amplitude α , for different measurement results $x_c = 0$, $x_b = 3$ (red), 4 (green), 5 (blue), and 6 (purple). The fidelity and amplitude, represented by the marked points, are respectively given by $\{F_a, \alpha\} \approx \{0.98, 1.2\}$, $\{0.97, 2.4\}$, $\{0.95, 3.2\}$, and $\{0.92, 4\}$. (b) The dependence of the Wigner negativity \mathcal{N}_a , the purity P_a and macroscopic quantum superposition \mathcal{M}_a of the state $\hat{\rho}_a^{\text{con}}$ on the measurement outcomes x_b , for $x_c = 0$. The interaction time $\alpha_p \chi^{(3)} t = 0.3$ and pump amplitude $\alpha_p = \sqrt{10}$.

and [56]

$$\mathcal{M}_a \equiv \frac{\pi}{2} \int W(\beta, \beta^*) \left(-\frac{\partial^2}{\partial \beta \partial \beta^*} - 1 \right) W(\beta, \beta^*) d^2 \beta. \quad (6)$$

We see that the nonclassicality has a peak around $x_b \approx 5$ since the optimal fidelity decreases as x_b increases. The macroscopicity still increases with the increasing of x_b . In addition, as shown from the time evolution of the optimal fidelity F_a^{max} , with respect to the cat-state amplitude α , and the negativity \mathcal{N}_a in Fig.4, for the fixed $x_b = 3$ the negativity becomes saturated with time, although the optimal fidelity decreases, since the amplitude α increases. At time $\alpha_p \chi^{(3)} t = 1$, $F_a^{\text{max}} \approx 0.83$, with respect to the cat state of amplitude $\alpha = 2.2$, and $\mathcal{N}_a \approx 0.58$. Therefore, the adjustable and large-amplitude optical cat states can be generated by homodyne detection for the present scheme. We note that small-size cat states (kitten) (the corresponding amplitude $\alpha \lesssim 1.6$) can only be realized via photon-subtraction detection [22–24].

We next study the two-mode state $\hat{\rho}_{bc}^{\text{con}}(x_a)$ of the modes b and c generated by homodyne on the quadrature \hat{X}_a of the mode a . In Fig.4 (a), we plot the fidelity F_{bc} of $\hat{\rho}_{bc}^{\text{con}}(x_a)$ with respect to a maximally entangled Bell state

$$|\psi\rangle_{\text{bell}} = \frac{1}{\sqrt{2}}(|0_b, 0_c\rangle + |1_b, 1_c\rangle). \quad (7)$$

The optimal fidelity $F_{bc} \approx 0.95$ around the outcome $x_a = 1$ at which the purity $P_{bc} \approx 0.99$ of the density matrix $\hat{\rho}_{bc}^{\text{con}}$, as shown in Fig.5 (a). Therefore, an approximate Bell entangled pure state $|\psi\rangle_{bc}^{\text{con}} \approx 0.817|0_b, 0_c\rangle + 0.531|1_b, 1_c\rangle$ is generated via homodyne detection. Such qubit entanglement is essential for scalable photonic quantum devices [57]. In Fig.5 (b), the negativity \mathcal{N}_{bc} of the Wigner function of

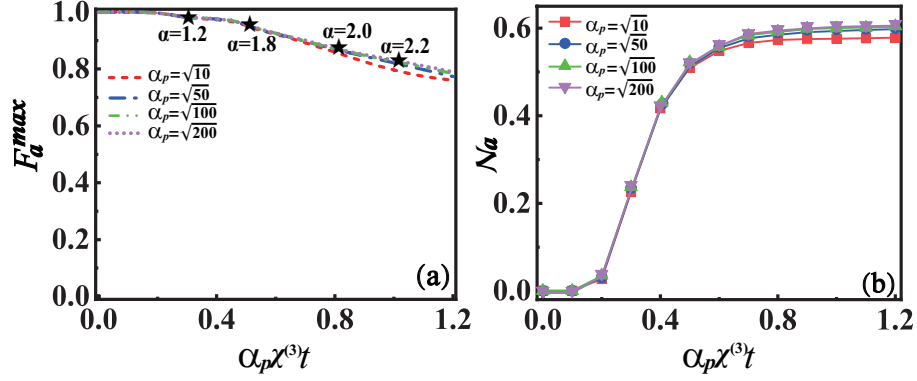


Figure 4. The time dependences of the optimal fidelity F_a^{\max} over different cat-state amplitudes α in (a) and the negativity \mathcal{N}_a of the state $\hat{\rho}_a^{\text{con}}$ in (b), for fixed measurement outcomes $x_b = 3$ and $x_c = 0$. The marked stars denote the optimal fidelity and the amplitude $\{F_a^{\max}, \alpha\} \approx \{0.98, 1.2\}, \{0.96, 1.8\}, \{0.87, 2.0\}$ and $\{0.83, 2.2\}$.

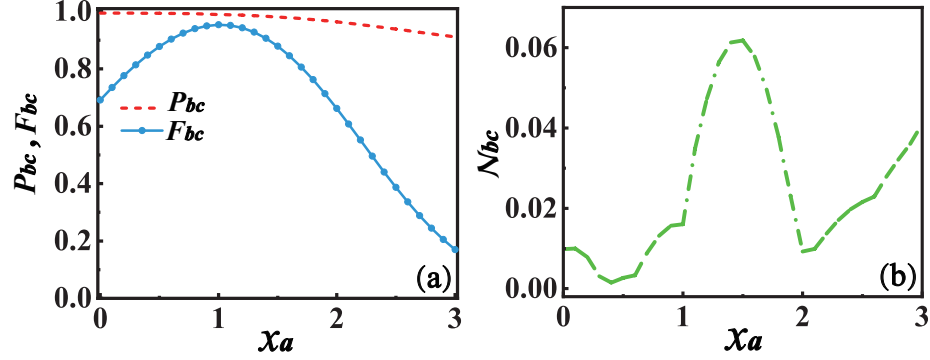


Figure 5. The purity P_{bc} and fidelity F_{bc} in (a) and the Wigner-function negativity \mathcal{N}_{bc} in (b) of the density matrix $\hat{\rho}_{bc}^{\text{con}}(x_a)$ as the function of the measurement result x_a . The interaction time $\alpha_p \chi^{(3)} t = 0.6$ and $\alpha_p = \sqrt{10}$.

$\hat{\rho}_{bc}^{\text{con}}(x_a)$ is plotted. It is shown the negativity is present, indicating genuine non-Gaussian nonclassicality. In addition, we see that the maximal negativity occurs in the vicinity of $x_a = 1.5$ at which the fidelity is not optimal. This is because that the probabilities of single- and two-photon states in the modes a and b increase as x_a arises from 1 to 1.5. At $x_a = 1.5$, the state becomes into a qudit entangle state: $|\psi\rangle_{bc}^{\text{con}} \approx 0.63|0_b, 0_c\rangle + 0.613|1_b, 1_c\rangle + 0.423|2_b, 2_c\rangle$, studied in Ref. [58].

4. Nonlinear quantum steering

The above results show that the measurements of normal linear quadratures of one or two modes can project the other modes into non-Gaussian nonclassical states. This is in fact due to the nonclassical correlations built up in the NTPSD process since the triplet's state $|\psi\rangle_{abc}(t)$ in the short-time regime $|\psi\rangle_{abc}(t) \approx |0_a, 0_b, 0_c\rangle + gt|1_a, 1_b, 1_c\rangle + \frac{g^2 t^2}{2}|2_a, 2_b, 2_c\rangle$, according to the Hamiltonian $\hat{H}_c = ig(\hat{a}^\dagger \hat{b}^\dagger \hat{c}^\dagger - \hat{a} \hat{b} \hat{c})$, for strong driving such that pump depletion can be neglected, where $g = \chi^{(3)} \bar{\alpha}_p$ with real pump amplitude

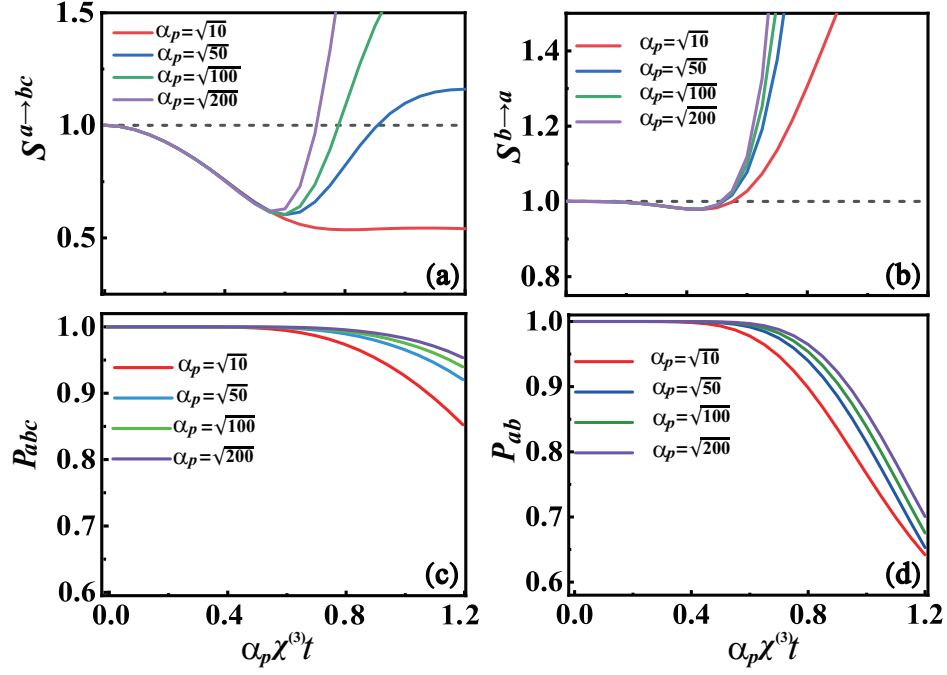


Figure 6. Time evolution of steering quantities $S^{a \rightarrow bc}$ in (a), $S^{b \rightarrow a}$, the purities P_{abc} and P_{ab} of the reduced state $\hat{\rho}_{abc}$ in (c) and $\hat{\rho}_{ab}^{\text{con}}$ with $x_c = 0$ in (d). The pump coherent-state amplitudes $\alpha_p = \sqrt{10}$, $\sqrt{50}$, $\sqrt{100}$, and $\sqrt{200}$.

$\bar{\alpha}_p$. Specifically, the correlations are quantum steerable, allowing us to steer desirable quantum states via remote measurement, in the spirit of the original EPR steering [42]. However, different from the latter which is linear and merely leads to conditional Gaussian states squeezing via homodyne detection [45], they are nonlinear. To reveal the nonlinear steering effects, let us at first define the generalized higher-order quadratures

$$\hat{X}_{bc} = \frac{\hat{b}\hat{c} + \hat{b}^\dagger\hat{c}^\dagger}{2}, \quad \hat{Y}_{bc} = \frac{\hat{b}\hat{c} - \hat{b}^\dagger\hat{c}^\dagger}{2i}. \quad (8)$$

The steering from the mode a to the group of the modes b and c can be characterized by the product of the inferred variances of the quadratures \hat{X}_{bc} and \hat{Y}_{bc} in the two-mode state $\hat{\rho}_{bc}^{\text{con}}$ from the measurements of the normal quadratures \hat{X}_a and \hat{Y}_a of the mode a [43], i.e.,

$$S^{a \rightarrow bc} = \frac{2\sqrt{\langle \Delta(\hat{X}_{bc}|x_a) \rangle_e \langle \Delta(\hat{Y}_{bc}|y_a) \rangle_e}}{\langle [\hat{X}_{bc}, \hat{Y}_{bc}] \rangle_e} < 1. \quad (9)$$

Here $\Delta(\hat{O}|r) \equiv \text{Tr}[\hat{\rho}_{bc}^{\text{con}}(r)\hat{O}^2] - [\text{Tr}[\hat{\rho}_{bc}^{\text{con}}(r)\hat{O}]]^2$ is the inferred variance of the operator $\hat{O} = \{\hat{X}_{bc}, \hat{Y}_{bc}\}$ for the two-mode states $\hat{\rho}_{bc}^{\text{con}}(r = x_a)$ and $\hat{\rho}_{bc}^{\text{con}}(r = y_a)$ conditioned on the outcomes $r = x_a$ and $r = y_a$ of the corresponding homodyne detection on \hat{X}_a and \hat{Y}_a , respectively. The symbol $\langle \cdot \rangle_e$ denotes the ensemble average over

all possible outcomes x_a and y_a . We have, for instance, $\langle \Delta(\hat{\mathcal{O}}|r) \rangle_e = \int dr P(r) \Delta(\hat{\mathcal{O}}|r)$, with the probability distribution $P(r)$, and similarly for the others. It can be seen from Eq.(9) that the higher-order variances seemingly violates the Heisenberg uncertainty relation, embodying the essence of the original EPR paradox [54]. Note that this is just a sufficient measure for the existence of nonlinear quantum steering. In addition, it can be implied from Eq.(9) that

$$\frac{\langle \Delta(\hat{X}_{bc}|x_a) \rangle_e}{\langle [\hat{X}_{bc}, \hat{Y}_{bc}] \rangle_e} < \frac{1}{2} \quad \text{or/and} \quad \frac{\langle \Delta(\hat{Y}_{bc}|y_a) \rangle_e}{\langle [\hat{X}_{bc}, \hat{Y}_{bc}] \rangle_e} < \frac{1}{2}, \quad (10)$$

showing that the nonlinear steering also means the presence of unconditional (or conditional) higher-order squeezing of the operators \hat{X}_{bc} or \hat{Y}_{bc} .

In Fig.6 (a) and (c), the time evolution of the steering quantity $S^{a \rightarrow bc}$ and the purity $P_{abc} \equiv \text{Tr}(\hat{\rho}_{abc}^2)$ of the reduced state $\hat{\rho}_{abc}$ is plotted for different pump coherent-state amplitude α_p . We see $S^{a \rightarrow bc} < 1$ in the short-time regime, showing nonlinear quantum steering from the mode a to the group of the modes b and c . Due to the symmetry among the triplets, it can therefore be concluded that the tripartite nonlinear steering can be built up among the triplets via the NTPSD process. As the amplitude α_p decreases, it takes longer time for $S^{a \rightarrow bc}$ to reach its minimal value (stronger steering), since the effective coupling $\chi^{(3)}\alpha_p$ decreases and it requires more time for accumulation. Also, the minima of $S^{a \rightarrow bc}$ become larger (weaker steering) as α_p increases, because of larger Fock space $\{|n_p\rangle\}$ occupied by the pump state, leading to less amount of nonclassicality. We note that in the experiment [41] strong coherent pump was employed to ensure large generation rate of the triplets. At the beginning of time development, the tripartite state is almost pure and it becomes mixed as the time continuously develops. The purity increases as the amplitude α_p increases, since this is closer to the case of classical treatment of the pump.

We further investigate the nonlinear steering between the two modes a and b in the conditional state $\hat{\rho}_{ab}^{\text{con}}(x_c)$ which is dependent on the outcome x_c . Similarly, the squared amplitudes of the mode a are defined by

$$\hat{X}_{a^2} = \frac{\hat{a}^2 + \hat{a}^{\dagger 2}}{2}, \quad \hat{Y}_{a^2} = \frac{\hat{a}^2 - \hat{a}^{\dagger 2}}{2i}. \quad (11)$$

We only consider the steering from the mode b to the mode a via homodyning the normal linear quadrature \hat{X}_b and \hat{Y}_b , quantified by $S^{b \rightarrow a}$ which is defined in the same way as Eq.(9) just by replacing the operators $\{\hat{X}_{bc}, \hat{Y}_{bc}\} \rightarrow \{\hat{X}_{a^2}, \hat{Y}_{a^2}\}$, with the variances of \hat{X}_{a^2} and \hat{Y}_{a^2} respectively in the states $\hat{\rho}_a^{\text{con}}(x_b, x_c)$ and $\hat{\rho}_a^{\text{con}}(x_b, y_c)$ and the ensemble average over the outcomes x_b and y_b .

In Fig.6 (b) and (d), the quantity $S^{b \rightarrow a}$ and the purity P_{ab} of the conditional state $\hat{\rho}_{ab}^{\text{con}}$ are respectively plotted for $x_c = 0$. It is shown that the steering can also exist in the transient regime but the degree of the steering is weaker than that of $S^{a \rightarrow bc}$. The purity of the conditional state is higher than that of the unconditional state $\hat{\rho}_{abc}$, due to the measurement enhancing the purity.

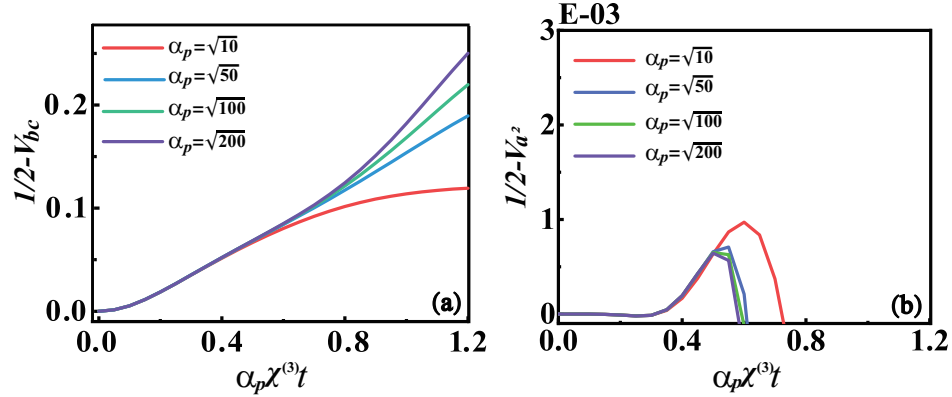


Figure 7. Time evolution of the conditional higher-order squeezing V_{bc} and V_{a^2} of the quadratures \hat{X}_{bc} for $x_a = 0$ in (a) and \hat{X}_{a^2} for both $x_b = 3$ and $x_c = 0$ in (b).

Finally, in Fig.7 (a) and (b) we plot the quantities

$$V_{bc} = \frac{\Delta(\hat{X}_{bc}|x_a)}{[\hat{X}_{bc}, \hat{Y}_{bc}]}, \quad V_{a^2} = \frac{\Delta(\hat{X}_{a^2}|(x_b, x_c))}{[\hat{X}_{a^2}, \hat{Y}_{a^2}]}.$$
 (12)

which depict the conditional higher-order squeezing of the quadratures \hat{X}_{bc} and \hat{X}_{a^2} when $V_{bc} < 1/2$ and $V_{a^2} < 1/2$. We see that compared to the nonlinear steering, the conditional higher-order squeezing exist in the longer-time regime because that the ensemble average in Eq.(10) is not performed. The squeezing of \hat{X}_{bc} is much larger than \hat{X}_{a^2} , since the former corresponds to stronger quantum steering.

In summary, we have studied the generation of optical quantum superpositions and nonlinear quantum steering effect in NTPSD. It is found that the remote generation of large-size single-mode optical Schrödinger cat states with high fidelity and two-mode Bell entangled states can be achieved by homodyne detection. This is enabled by the nonlinear steerable correlations among triplets, embodying by seeming violation of the Heisenberg uncertainty relation of the inferred variances of two noncommuting higher-order quadratures of downconverted modes, conditioned on the linear-quadrature measurements of another distant mode. Our results reveal non-Gaussian nonclassical features in NTPSD and would be useful for the fundamental tests of quantum physics and implementations of optical quantum tasks. Further study will include the investigation of nonclassical features of output fields for an intracavity NTPSD in the pulse and continuous pump regimes [59].

Acknowledgments

This work is supported by the National Natural Science Foundation of China (Nos.11674120 and 12174140) and the Fundamental Research Funds for the Central Universities (CCNU20TD003). Q.Y.He is supported by the National Natural Science Foundation of China (Grants No. 61675007, No. 11975026, and No. 61974067),

the Key R&D Program of the Guangzhou Province (Grant No. 2018B030329001), and the Beijing Natural Science Foundation (Grant No. Z190005).

Data availability statement

The data that support the findings of this study are available upon reasonable request from the authors.

References

- [1] E. Schrödinger 1935 Die gegenwärtige Situation in der Quantenmechanik *Naturwissenschaften* **23** 807
- [2] B. C. Sanders 1992 Entangled coherent states *Phys. Rev. A* **45** 6811
- [3] H. Jeong, W. Son, M. S. Kim, D. Ahn, and Č. Brukner 2003 Quantum nonlocality test for continuous-variable states with dichotomic observables *Phys. Rev. A* **67** 012106
- [4] F. De Martini and F. Sciarrino 2012 Colloquium: Multiparticle quantum superpositions and the quantum-to-classical transition *Rev. Mod. Phys.* **84** 1765
- [5] S. Haroche 2013 Nobel Lecture: Controlling photons in a box and exploring the quantum to classical boundary* *Rev. Mod. Phys.* **85** 1083
- [6] D. J. Wineland 2013 Nobel Lecture: Superposition, entanglement, and raising Schrödinger's cat* *Rev. Mod. Phys.* **85** 1103
- [7] A. Markus and K. Hornberger 2014 Testing the limits of quantum mechanical superpositions *Nat. Phys.* **10** 271
- [8] H. Jeong and M. S. Kim 2002 Efficient quantum computation using coherent states *Phys. Rev. A* **65** 042305
- [9] T. C. Ralph, A. Gilchrist, G. J. Milburn, W. J. Munro, and S. Glancy 2003 Quantum computation with optical coherent states *Phys. Rev. A* **68** 042319
- [10] A. P. Lund, T. C. Ralph, and H. L. Haselgrove 2008 Fault-Tolerant Linear Optical Quantum Computing with Small-Amplitude Coherent States *Phys. Rev. Lett.* **100** 030503
- [11] M. Bergmann and P. van Loock 2016 Quantum error correction against photon loss using multicomponent cat states *Phys. Rev. A* **94** 042332
- [12] S. Lee and H. Jeong 2013 Near-deterministic quantum teleportation and resource-efficient quantum computation using linear optics and hybrid qubits *Phys. Rev. A* **87** 022326
- [13] U. L. Andersen, J. S. Neergaard-Nielsen, P. van Loock, and A. Furusawa 2015 Hybrid discrete- and continuous-variable quantum information *Nat. Phys.* **11** 713
- [14] J. Joo, W. J. Munro, and T. P. Spiller 2011 Quantum Metrology with Entangled Coherent States *Phys. Rev. Lett.* **107** 083601
- [15] D. Leibfried, E. Knill, S. Seidelin, J. Britton, R. B. Blakestad, J. Chiaverini, D. B. Hume, W. M. Itano, J. D. Jost, C. Langer, R. Ozeri, R. Reichle, and D. J. Wineland 2005 Creation of a six-atom 'Schrödinger cat' state *Nature* **438** 639
- [16] K. G. Johnson, J. D. Wong-Campos, B. Neyenhuis, J. Mizrahi, and C. Monroe 2017 Ultrafast creation of large Schrödinger cat states of an atom *Nat. Commun.* **8** 697
- [17] A. Omran, H. Levine, A. Keesling, G. Semeghini, T. T. Wang, S. Ebadi, H. Bernien, A. S. Zibrov, H. Pichler, S. Choi, J. Cui, M. Rossignolo, P. Rembold, S. Montangero, T. Calarco, M. Endres, M. Greiner, V. Vuletic, and M. D. Lukin 2019 Generation and manipulation of Schrödinger cat states in Rydberg atom arrays *Science* **365** 570
- [18] C. Song, K. Xu, H. Li, Y. Zhang, X. Zhang, W. Liu, Q. Guo, Z. Wang, W. Ren, J. Hao, H. Feng, H. Fan, D. Zheng, D. Wang, H. Wang, and S. Zhu 2019 Generation of multicomponent atomic Schrödinger cat states of up to 20 qubits *Science* **365** 574

- [19] W. Leong, M. Xin, Z. Chen, S. Chai, Y. Wang, and S. Lan 2020 Large array of Schrödinger cat states facilitated by an optical waveguide *Nat. Commun.* **11** 5295
- [20] M. Brune, E. Hagley, J. Dreyer, X. Maâtre, A. Maali, C. Wunderlich, J. M. Raimond, and S. Haroche 1996 Observing the Progressive Decoherence of the “Meter” in a Quantum Measurement *Phys. Rev. Lett.* **77** 4887
- [21] J. S. Neergaard-Nielsen, B. M. Nielsen, C. Hettich, K. Mølmer, and E. S. Polzik 2006 Generation of a Superposition of Odd Photon Number States for Quantum Information Networks *Phys. Rev. Lett.* **97** 083604
- [22] A. Ourjoumtsev, R. Tualle-Brouri, J. Laurat, and P. Grangier 2006 Generating Optical Schrödinger Kittens for Quantum Information Processing *Science* **312** 83
- [23] A. Ourjoumtsev, H. Jeong, R. Tualle-Brouri, and P. Grangier 2007 Generation of optical ‘Schrödinger cats’ from photon number states *Nature* **448** 784
- [24] H. Takahashi, K. Wakui, S. Suzuki, M. Takeoka, K. Hayasaka, A. Furusawa, and M. Sasaki 2008 Generation of Large-Amplitude Coherent-State Superposition via Ancilla-Assisted Photon Subtraction *Phys. Rev. Lett.* **101** 233605
- [25] Feng-Xiao Sun, Sha-Sha Zheng, Y. Xiao, Qihuang Gong, Qiongyi He, and K. Xia 2021 Remote Generation of Magnon Schrödinger Cat State via Magnon-Photon Entanglement *Phys. Rev. Lett.* **127** 087203
- [26] T. Felbinger, S. Schiller, and J. Mlynek 1998 Oscillation and Generation of Nonclassical States in Three-Photon Down-Conversion *Phys. Rev. Lett.* **80** 492
- [27] K. Bencheikh, F. Gravier, J. Douady, J. A. Levenson, and B. Boulanger 2007 Triple photons: a challenge in nonlinear and quantum optics *C. R. Phys.* **8** 206
- [28] K. Banaszek and P. L. Knight 1997 Quantum interference in three-photon down-conversion *Phys. Rev. A* **55** 2368
- [29] T. Felbinger, S. Schiller, and J. Mlynek 1998 Oscillation and Generation of Nonclassical States in Three-Photon Down-Conversion *Phys. Rev. Lett.* **80** 492
- [30] M. V. Chekhova, O. A. Ivanova, V. Berardi, and A. Garuccio 2005 Spectral properties of three-photon entangled states generated via three-photon parametric down-conversion in a $\chi^{(3)}$ medium *Phys. Rev. A* **72** 023818
- [31] S. Agne, T. Kauten, J. Jin, E. Meyer-Scott, J. Z. Salvail, D. R. Hamel, K. J. Resch, G. Weihs, and T. Jennewein 2017 Observation of Genuine Three-Photon Interference *Phys. Rev. Lett.* **118** 153602
- [32] Y. Shen, S. M. Assad, N. B. Grosse, X. Y. Li, M. D. Reid, and P. K. Lam 2015 Nonlinear Entanglement and its Application to Generating Cat States *Phys. Rev. Lett.* **114** 100403
- [33] M. Miri 2020 Phase tristability in parametric three-photon down-conversion *Opt. Lett.* **45** 5546
- [34] Y. Zheng, O. Hahn, P. Stadler, P. Holmvall, F. Quijandría, A. Ferraro, and G. Ferrini 2021 Gaussian Conversion Protocols for Cubic Phase State Generation *PRX Quantum* **2** 010327
- [35] E. A. Rojas González, A. Borne, B. Boulanger, J.A. Levenson, and K. Bencheikh 2018 Continuous-Variable Triple-Photon States Quantum Entanglement *Phys. Rev. Lett* **120** 043601
- [36] T. Felbinger, S. Schiller, and J. Mlynek 1998 Oscillation and Generation of Nonclassical States in Three-Photon Down-Conversion *Phys. Rev. Lett* **80** 492
- [37] A. Agustí, C. W. Chang, F. Quijandría, G. Johansson, C. M. Wilson, and C. Sabín 2020 Tripartite Genuine Non-Gaussian Entanglement in Three-Mode Spontaneous Parametric Down-Conversion *Phys. Rev. Lett.* **125** 020502
- [38] D. Zhang, Y. Cai, Z. Zheng, D. Barral, Y. Zhang, M. Xiao, and K. Bencheikh 2021 Non-Gaussian nature and entanglement of spontaneous parametric nondegenerate triple-photon generation *Phys. Rev. A* **103** 013704
- [39] M. Walschaers 2021 Non-Gaussian Quantum States and Where to Find Them *PRX Quantum* **2** 030204
- [40] A. Cavanna, J. Hammer, C. Okoth, E. Ricardo, H. C. Ramirez, K. Palmett, A. B. U’Ren, M. H. Frosz, X. Jiang, N. Y. Joly, M. V. Chekhova, M. Corona, K. Garay-Palmett, and A. B. U’Ren

- 2020 Progress toward third-order parametric down-conversion in optical fibers *Phys. Rev. A* **101** 033840
- [41] C. W. Chang, C. Sabín, P. Forn-Díaz, F. Quijandría, A. M. Vadiraj, I. Nsanzineza, G. Johansson, and C. M. Wilson 2020 Observation of Three-Photon Spontaneous Parametric Down-Conversion in a Superconducting Parametric Cavity *Phys. Rev. X* **10** 011011
- [42] E. Schrödinger 1935 Discussion of Probability Relations between Separated Systems *Proc. Cambridge Philos. Soc.* **31** 555
- [43] M. D. Reid, P. D. Drummond, W. P. Bowen, E. G. Cavalcanti, P. K. Lam, H. A. Bachor, U. L. Andersen, and G. Leuchs 2009 Colloquium: The Einstein-Podolsky-Rosen paradox: From concepts to applications *Rev. Mod. Phys.* **81** 1727
- [44] H. M. Wiseman, S. J. Jones, and A. C. Doherty 2007 Steering, Entanglement, Nonlocality, and the Einstein-Podolsky-Rosen Paradox *Phys. Rev. Lett.* **98** 140402
- [45] Q. Y. He, Q. H. Gong, and M. D. Reid 2015 Classifying Directional Gaussian Entanglement, Einstein-Podolsky-Rosen Steering, and Discord *Phys. Rev. Lett.* **114** 060402
- [46] Q. Y. He, L. Rosales-Zarate, G. Adesso, and M. D. Reid 2015 Secure Continuous Variable Teleportation and Einstein-Podolsky-Rosen Steering *Phys. Rev. Lett.* **115** 180502
- [47] H. Tan, Y. Wei, and G. Li 2017 Building mechanical Greenberger-Horne-Zeilinger and cluster states by harnessing optomechanical quantum steerable correlations *Phys. Rev. A* **96** 052331
- [48] K. Sun, J. S. Xu, X. J. Ye, Y. C. Wu, J. L. Chen, C. F. Li, and G. C. Guo 2014 Experimental Demonstration of the Einstein-Podolsky-Rosen Steering Game Based on the All-Versus-Nothing Proof,” *Phys. Rev. Lett.* **113** 140402
- [49] S. Armstrong, M. Wang, R. Y. Teh, Q. Gong, Q. He, J. Janousek, H. A. Bachor, M. D. Reid, and P. K. Lam 2015 Multipartite Einstein-Podolsky-Rosen steering and genuine tripartite entanglement with optical networks *Nat. Phys.* **11** 167
- [50] S. Kocsis, M. J. W. Hall, A. J. Bennet, D. J. Saunders, and G. J. Pryde 2015 Experimental measurement-device-independent verification of quantum steering *Nat. Commun.* **6** 5886
- [51] Y. Xiao, X. J. Ye, K. Sun, J. S. Xu, C. F. Li, and G. C. Guo 2017 Demonstration of Multisetting One-Way Einstein-Podolsky-Rosen Steering in Two-Qubit Systems *Phys. Rev. Lett.* **118** 140404
- [52] X. Deng, Y. Xiang, C. Tian, G. Adesso, Q. He, Q. Gong, X. Su, C. Xie, and K. Peng 2017 Demonstration of Monogamy Relations for Einstein-Podolsky-Rosen Steering in Gaussian Cluster States *Phys. Rev. Lett.* **118** 230501
- [53] S. P. Walborn, A. Salles, R. M. Gomes, F. Toscano, and P. H. Ribeiro 2011 Revealing Hidden Einstein-Podolsky-Rosen Nonlocality *Phys. Rev. Lett.* **106** 130402
- [54] A. Einstein, B. Podolsky, and N. Rosen 1935 Can Quantum-Mechanical Description of Physical Reality Be Considered Complete? *Phys. Rev.* **47** 777
- [55] A. Kenfack and K. Życzkowski 2004 Negativity of the Wigner Function as an Indicator of Non-Classicality *J. Opt. B: Quantum Semiclass. Opt.* **6** 396
- [56] C. W. Lee and H. Jeong 2011 Quantification of Macroscopic Quantum Superpositions within Phase Space *Phys. Rev. Lett.* **106** 220401
- [57] J. W. Silverstone, R. Santagati, D. Bonneau, M. J. Strain, M. Sorel, J. L. áBrien, and M. G. Thompson 2015 Qubit entanglement between ring-resonator photon-pair sources on a silicon chip *Nat. Commun.* **6** 7948
- [58] A. Kowalewska-Kudłażyk, W. Leoński and J. Peřina Jr 2012 Generalized Bell states generation in a parametrically excited nonlinear couple *Phys. Scr. T.* **147** 014016
- [59] A. H. Kiilerich and K. Mølmer 2019 Input-Output Theory with Quantum Pulses *Phys. Rev. Lett.* **123** 123604